# A Scheme of Dynamic Initialization of the Boundary Layer in a Primitive Equation Model

YOSHIO KURIHARA AND ROBERT E. TULEYA

*Geophysical Fluid Dynamics Laboratory/NOAA, Princeton University, Princeton, N. J. 08540*

(Manuscript received 5 May 1977, in final form 3 August 1977)

ABSTRACT

A scheme of dynamic initialization of a primitive equation model is proposed with an emphasis on the dynamic adjustment in the boundary layer. The pre-initialization analysis is important since the restorative method is used in the subsequent dynamic initialization. The first phase of dynamic initialization is designed to establish a reasonable boundary layer structure. For this purpose, a time integration of the primitive equations is performed under a strong constraint such that all meteorological fields except momentum in the boundary layer are frozen. Use of an implicit form for the vertical diffusion term is recommended. The second phase is formulated to reduce the high-frequency noise in the final initialized field. Cyclic integration with a selective damping scheme is carried out under a restorative constraint.

The proposed scheme is applied to a case of simple zonal flow and the evolution of the boundary layer flow is shown. The scheme is also tested for a case of mature tropical cyclone. Starting from the wind data in the free atmosphere only, the initial condition of the model is derived. Subsequent time integration of the model compares favorably with the integration in a control experiment.

## 1. Introduction

To establish a proper initial state of a primitive equation (PE) model of the atmosphere is an important but complicated problem. The initial state may be regarded as dynamically adjusted, if 1) high-frequency noises do not prevail at the start of time integration of a model and also 2) the effects of forcing, such as those of surface friction and topography, are contained in the initial meteorological fields. The purpose of this paper is to propose a scheme which establishes a nearly adjusted initial state which includes the effects of surface friction.

It should be noted that the problem of initialization has to be treated consistently within the physical and mathematical framework of the model to be utilized for integration. Accordingly, the results of initialization are model-dependent. The initial state obtained may not be a very accurate reproduction of the actual state of the atmosphere. A realistic initial condition will be obtained by the improvement of the physics and the numerical aspects of the model.

The balance equation has been widely used to determine the initial fields of wind and mass in PE models. When high-frequency noise is excited initially by certain numerical imbalances, such noise can be suppressed with the use of a damping time integration scheme. The conventional form of the balance equation does not include a term expressing the effect of surface friction. This effect gradually evolves in a model during the course of integration. Krishnamurti (1969) showed that, starting from a balanced initial state, his model for the equatorial latitudes yielded a realistic flow field with convergence zones in 12–18 h after the initial time. In the numerical prediction experiment by Miyakoda *et al.* (1974), the divergent component was included in the initial wind. Nevertheless, the first three days were considered an initial adjustment period, during which two tropical storms weakened very rapidly. This may have been due to the lack of structure in the initial field which is needed for the maintenance of tropical disturbances.

The objective of dynamic initialization is to establish a dynamically adjusted field as the initial condition of a PE model rather than relying on its evolution from a crude initial state during subsequent integration. Miyakoda and Moyer (1968) proposed an initialization method in which a time-differencing scheme having a property of selective damping was used to perform a cyclic forward and backward integration repeatedly under a certain constraint on the velocity potential. An iteration method proposed by Nitta and Hovermale (1969) also uses a damping cyclic integration scheme but does not involve the abovementioned constraint. In these methods the mass or the wind field is recovered to the initially given value after each forward or backward forecast step. The results of the past

numerical tests show that either of the above two methods yields a large-scale vertical velocity field which agrees well with the solution of the so-called omega equation, i.e., the vertical motion required for the maintenance of the geostrophic balance relation.

Winninghoff (1973) discussed the difference between the physical natures of geostrophic adjustment and the adjustment to the heating and friction terms. In his initialization method, the geostrophic adjustment is treated by integrating the model alternately forward and backward six steps with a damping scheme. A restorative constraint is added after each iteration. Then the effects of heating and friction are included in a forward integration accompanied with the restorative procedure. In one of the experiments made by Mesinger (1972), the effect of friction is not treated separately but included only during the forward part of the iteration.

In addition to the analysis and initialization methods mentioned so far, the application of variational analysis (e.g., Sasaki, 1970), four-dimensional assimilation (e.g., Miyakoda *et al.*, 1976), and the method of adding a forcing term to a prognostic equation (e.g., Anthes, 1974) have been proposed in order to obtain a dynamically adjusted data set. Appropriate choice of the initialization method may be made by considering the nature of the problem, the scale of the phenomenon, the type of available data, the structure of the numerical model and other factors.

The various tactics of initialization cited above provided useful guides for the present study. This work was undertaken as a part of a numerical simulation study of atmospheric disturbances. It is well known that the so-called Ekman pumping plays an important role in the energetics of certain disturbances, especially those in the tropics. Therefore, special attention is given to the initialization of the planetary boundary layer part of a model. In Section 2 a strategy to construct the dynamically adjusted initial state is outlined. The numerical properties of the dynamic initialization scheme are investigated in Section 3. In Sections 4 and 5 the performance of the proposed scheme is demonstrated for the case of a simple zonal flow and that of a hurricane, respectively.

## 2. Strategy for analysis and dynamic initialization

A major task in the present study is to establish a dynamically adjusted initial condition in a model boundary layer. It is attempted to treat this problem with a method of dynamic initialization. This approach is useful in case an initial wind field in the boundary layer cannot be obtained directly from an observational analysis for various reasons and has to be derived by other means. It is assumed that a mass field can be observed or calculated in a physically sound fashion.

Before the start of dynamic initialization, a preinitialization field has to be prepared for a whole model. The field obtained in this analysis stage must be a reasonable one because certain variables are fixed or restored during the processes of the subsequent dynamic initialization stage. In this respect, the analysis of the mass field in the boundary layer is particularly important for the application of the proposed initialization scheme. The mass field in the boundary layer may be determined from the observational data if available. Otherwise, it may be obtained by utilizing the wind or mass field known at the top of the boundary layer. In the numerical examples in this paper, it is derived from the wind at about the 1 km level through extrapolation and the use of the reverse balance equation. At any rate, it is presumed in the present study that an accurate initial mass field can be obtained for the boundary layer at the analysis stage. In such a case, a mass field can be fixed during the dynamic initialization of the boundary layer wind. In the analysis of the free atmosphere, various conditions may be imposed on the data. In this paper, a balance relation is assumed. Given the wind field, the mass field is computed by the simplified reverse balance equation. If the balanced state is not a valid approximation of the actual fields, a different analysis principle has to be sought.

The present dynamic initialization scheme consists of two phases. In the first phase, the dynamical effect of surface friction is incorporated into the boundary layer where the mass field was specified at the analysis stage. This is done by making a forward integration of the model while anchoring the mass field everywhere and the momentum field above the boundary layer. With these constraints the fields in the free atmosphere determined at the analysis stage are preserved. In the boundary layer, the wind approaches a balanced state which includes the frictional effect. During this process, gravity waves are not excited as the mass field remains unchanged. The fixed momentum in the free atmosphere provides the upper boundary condition for the layer below. The first phase integration is continued until the momentum field in the boundary layer establishes a quasi-equilibrium state. The boundary layer wind thus obtained yields frictional mass convergence which can cause external gravity waves unless it is compensated for in the vertical net convergence. To avoid these waves, a small correction, usually less than 0.1 m $s^{-1}$, is made to the wind field in the free atmosphere after the first phase integration.

The second phase of dynamic initialization involves cyclic integration with a restorative-iterative technique (Nitta and Hovermale, 1969). The primary function of the proposed second phase of dynamic initialization in the present study is the suppression of possible noise due to slight imbalances between the mass and momentum fields at the end of the first phase. These imbalances may be caused by the approximations in solving the reverse balance equation or by the above-mentioned wind correction. Provided the imbalance is

small, it makes little difference whether the mass field or the rotational component of the wind is the restored field during the process of cyclic integration. Indeed, in some cases one may be able to skip the second phase entirely (e.g., Sundqvist, 1975). During the second phase it is also expected that the divergent wind field which is required for maintaining a balance condition may evolve. The boundary layer structure which was established in the previous phase of initialization should be practically unaffected by the cyclic integration in this phase.

On the other hand, if the mass and wind fields specified at the analysis stage are not in approximate balance, the second phase may serve the more vital function of geostrophic adjustment. In this case, the choice of variables to be restored should take the scale of the meteorological fields into account.

## 3. Numerical characteristics of the dynamic initialization scheme

As mentioned in Section 2, the dynamic initialization method in the present study consists of two phases of dynamical adjustments. The behavior of numerical schemes dealing with each adjustment is investigated in this section. Although the analysis will be made with respect to an equation which includes the frictional effect in a simple form, the proposed algorithm of initialization can be applied without difficulty to a model which incorporates the frictional effect in a fairly complicated form. It should be remarked that despite the time integrations involved in the dynamical adjustments, the actual time level for the model remains unchanged during the dynamic initialization stage.

### *a. Construction of planetary boundary layer*

By ignoring the advective term for simplicity, the momentum equation with a friction term may be written in the $\sigma$ coordinate system (Phillips, 1957) as

$$\frac{\partial \mathbf{V}}{\partial t}=-f\mathbf{k}\times\mathbf{V}-\left(\nabla\Phi+\frac{RT}{p_*}\nabla p_*\right)-c\mathbf{V}, \qquad (3.1)$$

where $\mathbf{V}$ is the horizontal wind with the components $u$ and $v$, $\mathbf{k}$ the vertical unit vector, $\Phi$ the geopotential ($gz$), $p_*$ the surface pressure, $c$ represents the inverse of time scale for frictional damping and the other symbols have standard meanings. The three terms on the right-hand side of (3.1) represent the Coriolis force, the pressure gradient force and the frictional force, respectively. If a balanced wind $\mathbf{V}_B$ exists for a given pressure field, it should satisfy the equation

$$\frac{\partial \mathbf{V}_B}{\partial t}=-f\mathbf{k}\times\mathbf{V}_B-\left(\nabla\Phi+\frac{RT}{p_*}\nabla p_*\right)-c\mathbf{V}_B, \qquad (3.2)$$

where the left-hand side is actually zero by definition. Subtracting (3.2) from (3.1) yields

$$\frac{\partial}{\partial t}(\mathbf{V}-\mathbf{V}_B)=-f\mathbf{k}\times(\mathbf{V}-\mathbf{V}_B)-c(\mathbf{V}-\mathbf{V}_B). \qquad (3.3)$$

Eq. (3.3) indicates that, if the time integration of (3.1) is carried out with the mass field fixed, $\mathbf{V}$ will approach $\mathbf{V}_B$ since the vector $\mathbf{V}-\mathbf{V}_B$ is continuously damped while it rotates (clockwise in the Northern Hemisphere) with the period $2\pi/f$. Note that the obtained wind $\mathbf{V}_B$ is not dependent on the wind assumed at the start of the time integration.

Based on the above argument, a scheme to establish a boundary layer structure in a numerical model may be proposed. This scheme involves a time integration of primitive equations under the constraint that all the meteorological fields except momentum below a certain level are frozen at the pre-initialization values during the period of integration. As the mass field is fixed, there exists no gravity wave in the model. Accordingly, a large time step can be taken to make the integration.

Numerical methods suitable for the abovementioned integration are discussed below. For this purpose, the equation in the form

$$\frac{\partial h}{\partial t}=-iah-ch \qquad (3.4)$$

is used. The parameters $a$ and $c$ are related to the frequency of oscillation and the rate of frictional damping, respectively. The above equation reduces to (3.3) if $h=(u-u_B)+i(v-v_B)$ and $a=f$. For convenience, $b$ and $d$ are defined as

$$b=a\Delta t, \quad d=c\Delta t, \qquad (3.5)$$

where $\Delta t$ is a time increment for the integration.

Integration of (3.4) may be made in a split form. First, the change due to the frictional effect only is considered. This change ($\Delta h$) is estimated for a period $2\Delta t$, while the leapfrog scheme will be used in dealing with the other term. If computed explicitly, the change becomes

$$\Delta h=-2dh^{n-1},$$

where a superscript denotes the time-step number ($n$ for the latest time level). In case of a backward implicit estimate, the change is

$$\Delta h=-\frac{2d}{1+2d}h^{n-1},$$

because $\Delta h=-2dh'$ where $h'=h^{n-1}+\Delta h$. After adding $\Delta h$ to $h^{n-1}$, the other term in (3.4) is treated by the leapfrog method to obtain $h^{n+1}$:

$$h^{n+1}=(h^{n-1}+\Delta h)-2ibh^n. \qquad (3.6)$$

In general, $h^{n+1}$ is related to $h^n$ by the amplification

factor $\lambda$, i.e.,

$$h^{n+1}=\lambda h^n. \tag{3.7}$$

There exist two $\lambda$'s for (3.6)—one for the physical mode and another for the computational mode. The scheme (3.6) is computationally stable when the amplification rate $|\lambda|$ of both modes is less than unity. In Fig. 1 $|\lambda|$ of the physical mode for the case of the implicit estimate of the friction term is shown as a function of $b$ and $d$. It is reasonable to see that the damping rate increases with $d$. For a given $d$, there is a critical value of $b=b_c=[1/(1+2d)]^{\frac{1}{2}}$. If $b<b_c$, then the damping rate of the physical mode does not depend on $b$, i.e., $|\lambda|=b_c$. Also, if $b>(1+d)/(1+2d)$, then $|\lambda|$ of the computational mode exceeds unity. The computationally unstable domain is shaded in Fig. 1. There is therefore a limit to the increment $\Delta t$ for making a stable integration.

Fig. 2 shows the result of a similar analysis of $|\lambda|$ for the case of leapfrog integration with the frictional term in an explicit differencing form. The physical mode is completely eliminated for $d=0.5$. When $d>0.5$, damping is weaker as $d$ increases. This is unreasonable and undesirable. The computationally stable area is smaller than the previous case because of greater amplification of the computational mode. As a result of the above analysis, it is recommended that the vertical diffusion terms in the prognostic equations be treated with an implicit scheme.

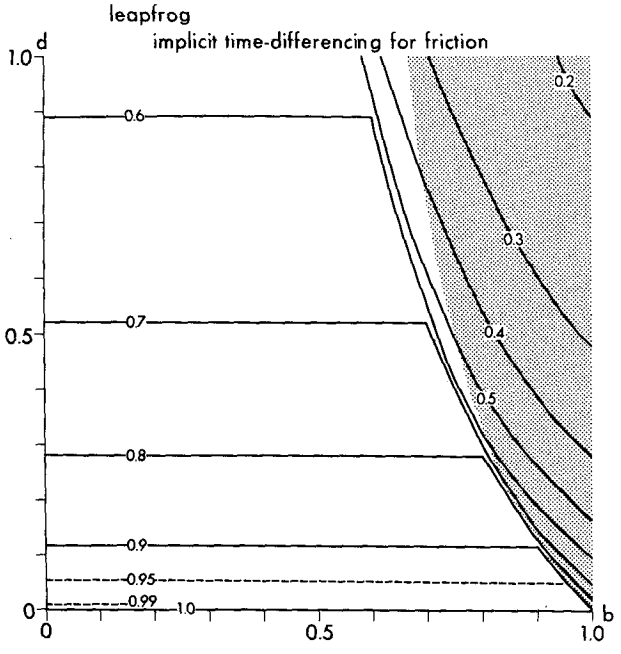


FIG. 1. Amplification rate of the physical mode for the leapfrog scheme (3.6). The friction term is treated by implicit differencing. The parameters $b$ and $d$ represent frequency and frictional effects, respectively. The computational mode makes the scheme computationally unstable in the shaded area.

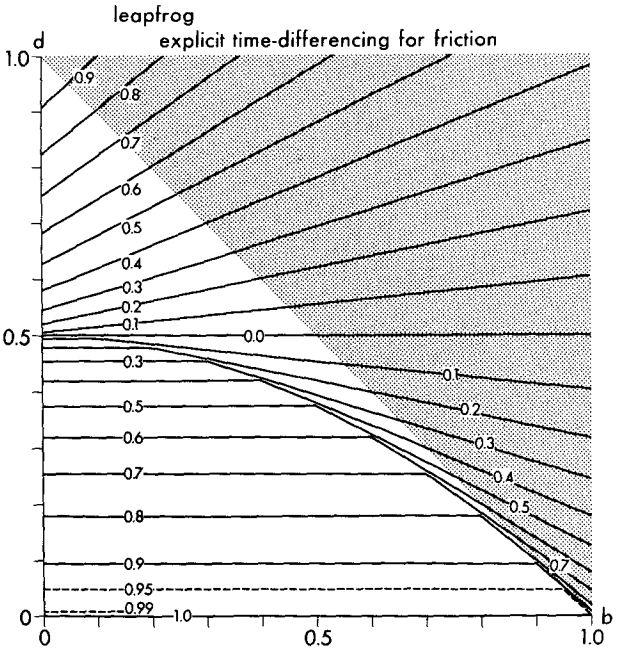


FIG. 2. As in Fig. 1 except that friction term is treated by explicit differencing.

The time integration of (3.4) may also be made with the Euler-backward method. According to the analysis of $|\lambda|$ in this case, the numerical damping rate is strongly influenced by the frequencies represented by the parameter $b$ even though the damping parameter $d$ is fixed. Again, it is recommended that an implicit estimate of the vertical diffusion term be used.

In the numerical examples in the following two sections, the momentum equation will be integrated in the first phase of initialization by applying the implicit scheme to the separated vertical diffusion term, the forward scheme to the horizontal diffusion term and the leapfrog scheme to the other terms.

### *b. Suppression of high-frequency noise*

As mentioned in Section 1, it has been demonstrated that cyclic (i.e., forward and backward) integrations with a selective damping scheme can suppress high-frequency noise. Specifically, one cycle for the case of (3.4) may be written, with the use of (3.5), as

$$\left.\begin{aligned} h_F^*&=h^n-ibh^n+(\Delta h)_F\\ h_F&=h^n-ibh_F^*+(\Delta h)_F \end{aligned}\right\}, \tag{3.8}$$

$$\left.\begin{aligned} h_B^*&=h_F+ibh_F-(\Delta h)_B\\ h^{n+1}&=h_F+ibh_B^*-(\Delta h)_B \end{aligned}\right\}, \tag{3.9}$$

where superscript denotes iteration number. If the frictional effect is separated from the other term and

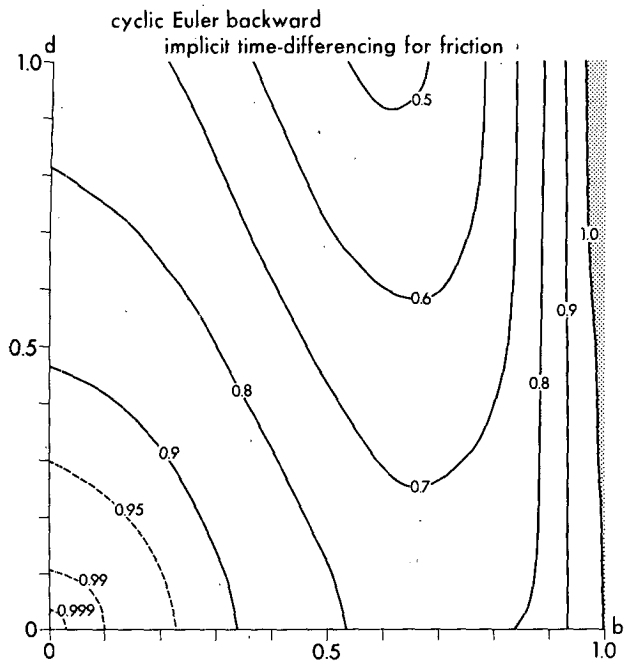


FIG. 3. Amplification rate for the cyclic Euler-backward scheme [Eqs. (3.8) and (3.9)]. The friction term is treated by implicit differencing. The computationally unstable area is shaded.

estimated in an implicit manner, $\Delta h$ is expressed as

$$(\Delta h)_F = -\frac{d}{1+d}h^n, \quad (\Delta h)_B = -\frac{d}{1+d}h_F.$$

The amplification factor $\lambda = h^{n+1}/h^n$ for the above case can be obtained easily. Fig. 3 shows the distribution of $|\lambda|$ on the $b$-$d$ domain. For a fixed value of $d$ the dependency of $|\lambda|$ on $b$ is large. Accordingly, with a proper choice of value for $\Delta t$, selective damping of high-frequency waves can be expected.

A scheme of cyclic integration is suitable only for the second phase of the dynamic initialization. If it were used during the first phase, the wind speed in the boundary layer would still approach a fairly reasonable value. However, the desired veering of wind would be achieved very slowly as the rotations of the wind vector at the forward and the backward steps almost cancel each other.

In Sections 4 and 5, the momentum equation will be treated everywhere with a scheme similar to (3.8) and (3.9) during the second phase of the dynamic initialization. It includes the vertical diffusion term formulated in an implicit form. Equations for the temperature and the mixing ratio of water vapor, including the effect of moist convection, are also integrated in the same way except that the original temperature and moisture fields are restored after both the forward and the backward steps, i.e., twice in one cycle. As mentioned before, this restoration procedure may be allowed when a nearly balanced state is expected between the mass and wind field at the start of the initialization of the second phase.

## 4. Example 1: Initialization of a simple zonal flow

In this section, the proposed initialization scheme is utilized for a simple zonal flow. The evolution and structure of the boundary layer are investigated.

The numerical model which resolves the boundary layer is essentially the same as the model used earlier for the simulation of tropical cyclones (Kurihara and Tuleya, 1974). A brief description of the model follows. It is an 11-level primitive equation model, using $\sigma$-coordinates. The lowest four levels are placed at $\sigma = 0.992$, 0.977, 0.950 and 0.895. The approximate heights of these levels are 68, 196, 435 and 926 m, respectively. Subgrid-scale processes are parameterized and incorporated in the model. The horizontal diffusion effect is computed with the use of a nonlinear diffusion coefficient. Exchanges of momentum and energy at the lower boundary are estimated in the Monin-Obukhov framework. Vertical diffusion due to mechanical turbulence is dependent on the Richardson number. Both dry and moist convection effects are treated by a convective adjustment method. The finite-difference equations are formulated with the box method. The grid system to be used in this section has a latitudinal spacing of 2°. The grid domain covers 40°S–40°N with open lateral boundaries.

In this example, as well as in the next, the reverse balance equation was used at the analysis stage. The balance equation in the $\sigma$-coordinate system was derived and discussed by Sundqvist (1975). Its form in spherical coordinates is

$$G(u,v) = \nabla^2\Phi + \frac{\partial}{\alpha\partial\lambda}\left(\frac{RT}{p_*}\frac{p_*}{\alpha\partial\lambda}\right) + \frac{\partial}{\alpha\partial\phi}\left(\cos\phi\frac{RT}{p_*}\frac{\partial p_*}{a\partial\phi}\right), \quad (4.1)$$

where

$$G(u,v) = 2J_{\lambda,\phi}(u,v) + f\zeta - u\beta - \frac{\partial}{\alpha a\partial\phi}[(u^2+v^2)\sin\phi]. \quad (4.2)$$

Except for the ordinarily used symbols, $\alpha$ in the above equations is equal to $a\cos\phi$, $\Phi(=gz)$ is geopotential, and vorticity and two operators are defined by

$$\left.\begin{aligned} \zeta &= \frac{\partial v}{\alpha\partial\lambda} - \frac{\partial u\cos\phi}{\alpha\partial\phi} \\ \nabla^2 &= \frac{\partial^2}{\alpha^2\partial\lambda^2} + \frac{\partial}{\alpha\partial\phi}\left(\cos\phi\frac{\partial}{a\partial\phi}\right) \\ J_{\lambda,\phi}(u,v) &= \frac{1}{\alpha a}\left(\frac{\partial u}{\partial\lambda}\frac{\partial v}{\partial\phi} - \frac{\partial u}{\partial\phi}\frac{\partial v}{\partial\lambda}\right) \end{aligned}\right\}. \quad (4.3)$$

When (4.1) is used to solve the mass field, i.e., $p_*$ and $\Phi$, for a given wind field, it is called the reverse balance equation. In specifying the wind field, it should be taken into consideration that (4.1) does not include the frictional effect which, at the top of the boundary layer, is presumably small. In this study, the wind in the boundary layer was taken to be equal to the wind at $\sigma=0.895$. This fictitious, frictionless flow is used to solve the reverse balance equation for the mass field in the boundary layer. The mass field thus obtained will be reasonable if the boundary layer is nearly barotropic. Since the temperature is related to $\partial\Phi/\partial\sigma$ by the hydrostatic relation, (4.1) represents a three-dimensional problem. However, if a prescribed temperature $T_0$ is substituted for $T$ in (4.1), the mathematical complexity can be reduced drastically. Particularly, if $T_0$ is treated as a function of $\sigma$ only, the following simplified equations of the Poisson type for $\ln p_*$ and $\Phi$ are derived:

$$RT_{0*}\nabla^2 \ln p_* = G_* - g\nabla^2 z_*, \qquad \sigma=1, \quad (4.4)$$

$$\nabla^2\Phi = G - (T_0/T_{0*})(G_* - g\nabla^2 z_*), \qquad \sigma<1, \quad (4.5)$$

where an asterisk denotes a value at the earth's surface. Surface-height $z_*$ is zero in the present study. If the observational data of $p_*$ are available, Eq. (4.4) may be used inversely to estimate the right-hand side. Once $\Phi$ is determined from (4.5), then $T$ is obtained from the hydrostatic relation. As pointed out by Miyakoda and Moyer (1968), a finite-difference formulation of the balance equation must be consistent with the numerical scheme of the prognostic equations to be used later in the dynamic initialization and the forward integration.

In the present example, the initial meteorological data were the wind data representing a simple zonal flow. The specified flow was from the east with a constant angular velocity, giving the speed of 15.8 m s$^{-1}$ at the equator. The mass field was obtained by solving the simplified reverse balance equation. In doing so, $p_*$ at the equator was set to 1010 mb. Also $T_0$ was taken from a climatological mean for the tropics. Values of $\Phi$ computed from $T_0$ were assigned to the equator.

In the first phase of the dynamic initialization, the time integration was performed with a time increment of 15 min, except that the Euler-backward scheme was used at the start of integration. Only the momentum at the lowest three levels was allowed to change with time. All other quantities remained unaltered. Fig. 4 shows the time variation of wind $\mathbf{V}(u,v)$ at $\sigma=0.992$ and at 20°N. The dashed line traces the evolution of the wind vector point with time. The wind clearly approaches a certain frictionally balanced flow $\mathbf{V}_B$. The time change of $\mathbf{V}-\mathbf{V}_B$ is in agreement with what is implied by (3.3); namely, the vector $\mathbf{V}-\mathbf{V}_B$ makes a clockwise loop with an inertial period which is about 35 h at 20°N, while it undergoes frictional damping. After a 40 h integration, the deflection angle of wind from the initial easterly direction became 23°, and the speed was reduced to about 70% of the initial value. The integration may be terminated at about one day since the change after that is very little.

Fig. 5 shows the boundary layer structure established in the model after 40 h of evolution. A dashed line connects the points of the wind vector at $\sigma=0.992$ at different latitudes. Wind vectors at 10, 20 and 30°N are shown by thin solid lines. The wind deflection angle increases from zero at the equator to 24° at 3°N, north of which the angle variation is rather small. The ratio of wind speed at $\sigma=0.992$ to that at $\sigma=0.895$ is smaller at the lower latitudes. The northerly component of wind increases from the equator to 10°N. This causes frictional mass convergence at the equator. A very weak meridional correction was introduced in the free atmosphere wind field in order to compensate for this convergence after the integration was terminated. The correction amount $\mathbf{D}$ was obtained from the condition

$$\int_0^1 \nabla\cdot p_*(\mathbf{V}+\mathbf{D})d\sigma = 0. \qquad (4.6)$$

In this paper, $\mathbf{D}$ was assumed to be independent o- height in the free atmosphere and vanish at the boundf ary layer. Thick solid lines in Fig. 5 are the hodographs of wind in the boundary layer at 10, 20 and 30°N. Those patterns resemble that of the Ekman spiral. The

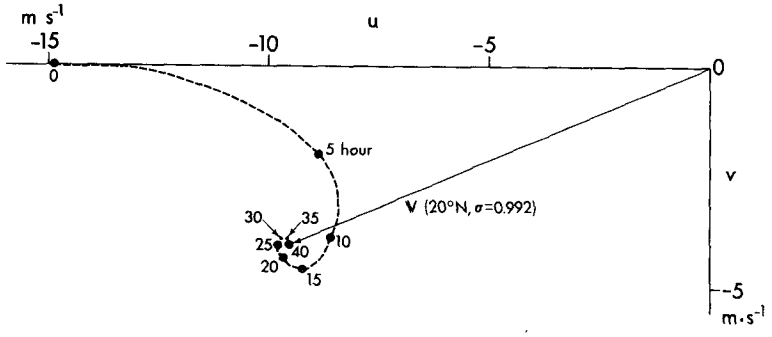


FIG. 4. Evolution of the wind at $\sigma=0.992$ and at 20°N during the first phase of dynamic initialization. The point of the wind vector is traced by the dashed line.

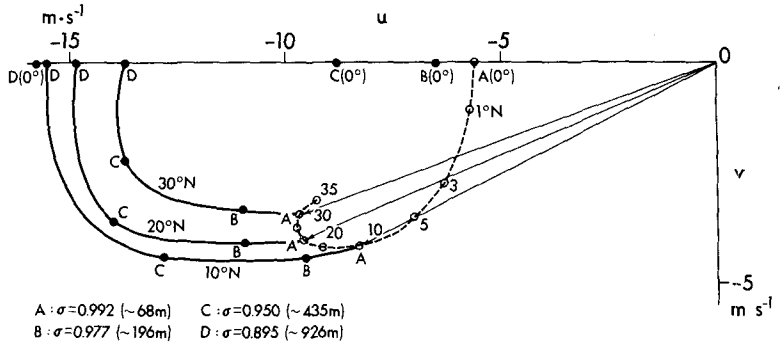


FIG. 5. Boundary layer structure established by the dynamic initialization. The dashed line connects the points of the wind vectors at $\sigma=0.992$ at different latitudes. Winds at this level at 10, 20 and 30°N are indicated by thin solid arrows. The hodographs for those latitudes are shown by thick solid lines. Winds at the equator, having $u$ component only, are also shown.

winds at the different levels at the equator are also plotted. The wind there is zonal and increases with height. Note that, in the present study, the top of the boondary layer is set at $\sigma=0.895$, i.e., at a height of uabut 1 km.

The second phase of dynamic initialization was made through the cyclic integrations. The total number of time steps was equivalent to that in a 4 h integration. The wind change during this integration was very small and the boundary layer structure was well preserved. Latitudinal distributions of the zonal wind component, relative vorticity and divergence at the end of the initialization obtained for this particular case are presented in Fig. 6. It is seen that the downward decrease of zonal wind speed is largest at the equator. Between the equator and about 10°N, the flow near the surface is characterized by convergence and positive relative vorticity, while that at the top of boundary layer is characterized by nondivergence and negative relative vorticity. The present results indicate that a surface convergence zone may form at the equator if a simple zonal flow and uniform sea surface temperature are specified. In reality, however, the equatorial flow is more complicated than this.

## 5. Example 2: Initialization of a hurricane

An initialization of a tropical cyclone model using the proposed scheme is attempted in this section. An initial field is obtained by utilizing only a part of the

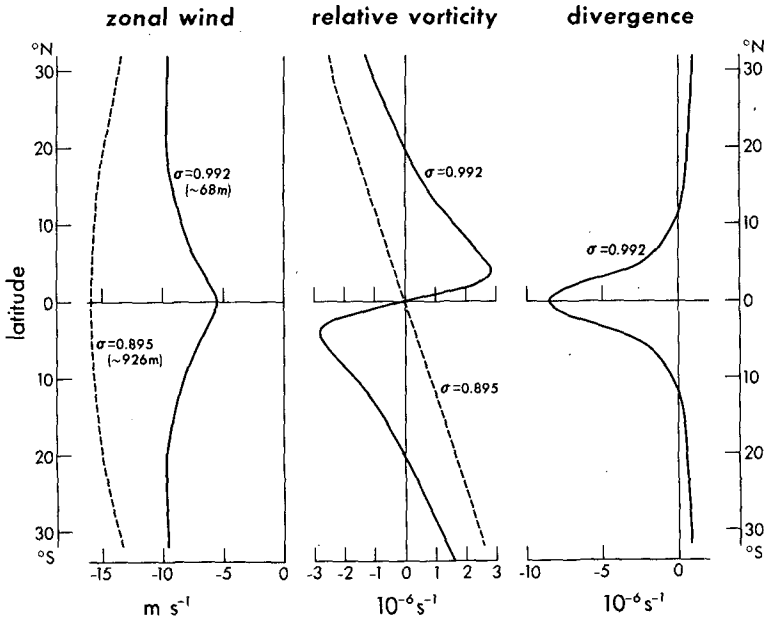


FIG. 6. Latitudinal distributions of zonal component of wind, relative vorticity and divergence at the end of the dynamic initialization.

data at hour 80 of the control experiment. Here, the control experiment refers to the simulation experiment of Kurihara and Tuleya (1974). Furthermore, starting from the obtained field, a time integration of the model is made beyond hour 80 and the result is compared against that of the control experiment for the corresponding period. The model used in this example and that in the control experiment is the same. Its main features were described in the previous section.

At first, the wind data at and above the level $\sigma=0.895$ only were taken from the data set at hour 80 of the control experiment. All other quantities except relative humidity were hypothetically considered unavailable. As mentioned before, if the balance relation without frictional effects is applied to the boundary layer, the wind there should be the fictitious wind which would be observed in the absence of surface friction. In this example, the wind at $\sigma=0.895$ was simply assigned to the lowest three levels. After that, the initial analysis proceeded as follows:

1) Compute relative vorticity at each level from the given wind.
2) Obtain streamfunction by relaxation.
3) Recompute the wind from the streamfunction.
4) Solve the simplified reverse balance equation to obtain the nearly balanced mass field, $p_*$ and $\Phi$.
5) Compute $T$ by using the hydrostatic relation.
6) Compute the mixing ratio of water vapor from the specified relative humidity.

In step 4, $T_0$ had to be known [see Eqs. (4.4) and (4.5)]. The average temperature at the 2000 km radius from the storm center of the control experiment at hour 80 was used for this purpose. This temperature is about the same as the actual mean temperature of the hurricane environment. The mean surface pressure at the 2000 km radius also was obtained from the control experiment. This value as well as the geopotential derived from $T_0$ were specified at the 2000 km radius as the boundary condition for solving the simplified reverse balance equation. The mass field thus analyzed agrees well with that of the control case, except in a very small area near the center where the analyzed $p_*$

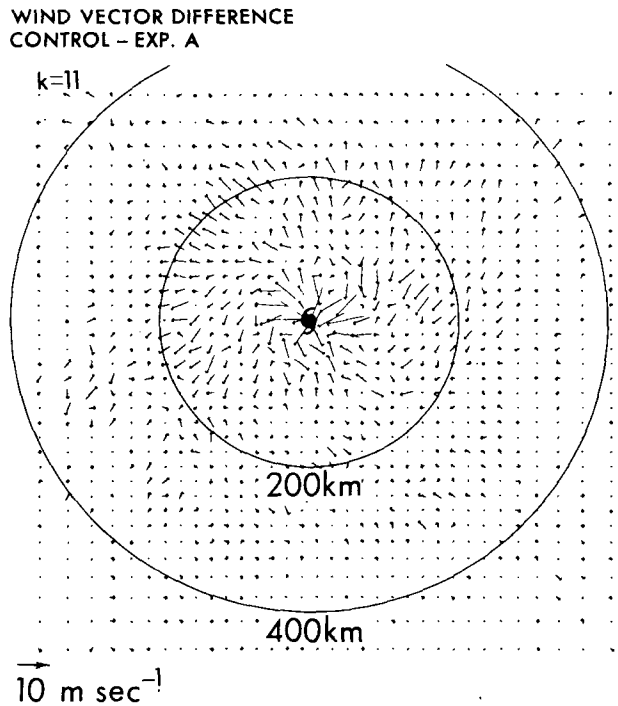


FIG. 7. Wind vector difference at $\sigma=0.992$ after 1 h integration: the control experiment minus Experiment A.

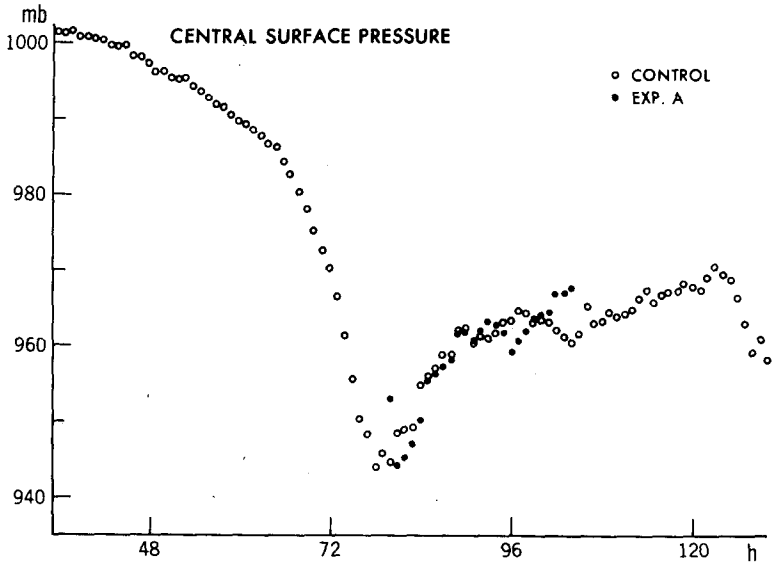


FIG. 8. Time variation of central surface pressure for the control experiment (open circles) and for Experiment A (dots).

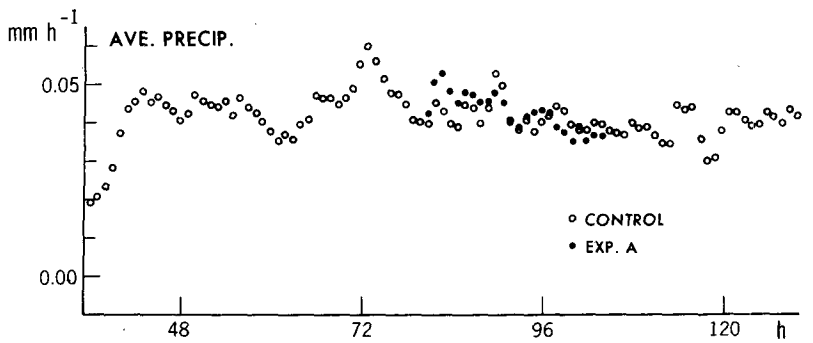


FIG. 9. Time variation of area mean precipitation for the control experiment (open circles) and for Experiment A (dots).

was higher by 8 mb. In step 6, the relative humidity at hour 80 of the control experiment was utilized.

The first phase of dynamic initialization was made by the time integration of the model for a period of 20 h with a scheme similar to that used in the previous example. A reasonable wind field was established in the boundary layer. After the integration, a weak divergent wind correction was added to the free atmosphere to compensate for the boundary layer convergence. The second phase of initialization was made by cyclic integration for a period equivalent to 2 h. During this phase, the surface wind decreased slightly, perhaps because the approach of the boundary layer wind to a balanced flow was not quite complete at the end of the first phase. Although the second phase initialization was carried out, it seems that high-frequency noise in the model was not appreciable at the start of this phase since the abovementioned divergent wind addition to the balanced wind was very small.

The marching integrations of the model beyond hour 80 were made starting from two different initial conditions. For Experiment A, the initial field was prepared as described above. For Experiment B, the dynamic initialization was omitted, and the initial field was provided from the analysis stage.

Fig. 7 shows the wind vector difference between the control experiment and Experiment A at the lowest level at hour 81, i.e., at 1 h after the start of integration. Beyond 200 km radius the difference is very small. The establishment of boundary layer flow by the proposed method seems to be acceptable. Within the inner region an asymmetric difference of several meters per second is seen. This may be ascribed to the fact that the mass field was derived at the analysis stage from the simplified reverse balance equation which did not include the effect of divergence. It is also possible that the difference was caused by an unbalanced component of wind. Experiment A was continued for 24 h. Time variations of central surface pressure and of the domain-averaged precipitation are compared, respectively, in Figs. 8 and 9, against those of the control experiment. It is encouraging that Experiment A more or less reproduced the control experiment's results. The wind vector difference at the lowest level at hour 81, the control experiment minus Experiment B, is presented in Fig. 10. It is clearly shown that the boundary layer inflow is considerably weaker in Experiment B at 1 h integration when the marching started from the balanced wind. This experiment was continued for several hours. A tendency for the storm to approach a state close to the control experiment was observed in the later period. It has to be noted that the initial wind in the boundary layer in Experiment B was azimuthal and much stronger than the control case. Accordingly, inward deflection of wind after several hours of integration makes generation of kinetic energy large enough to maintain the storm. Another reason why the storm did not deteriorate in Experiment B is that the large

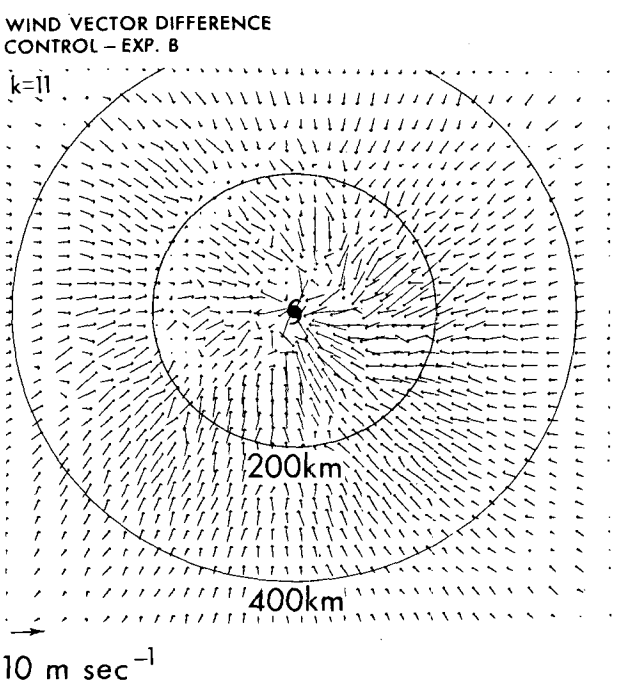


FIG. 10. As in Fig. 7 except for the control experiment minus Experiment B.

relative humidity near the storm center was specified from the control experiment. It is speculated that the boundary layer inflow at the initial time may be more crucial in weak disturbances.

## 6. Summary and remarks

A dynamic initialization scheme to establish the flow field in the boundary layer of a primitive equation model is proposed. This scheme can be utilized in or added to other initialization schemes. First, the mass field in a boundary layer has to be given from observation or calculated from the wind field aloft. Then a dynamically adjusted boundary layer is obtained by integration of the momentum equation under a dynamical constraint. It is recommended that the vertical diffusion term be treated in an implicit manner. The boundary layer mass convergence which results is compensated by a forced weak divergence in the free atmosphere. In the following phase of initialization, which may be omitted in some cases, possible high-frequency noise is suppressed by cyclic integration with a selective damping scheme to yield the initial condition from which the forward integration of a model can proceed smoothly.

The proposed scheme was applied to the cases of a simple zonal flow and a mature tropical cyclone. Promising results were obtained. In these numerical examples, the ocean with a constant surface temperature was assumed at the lower boundary. Nonuniform boundary conditions, such as a variable surface temperature or a variable surface roughness condition, can be easily treated by the proposed scheme of dynamic initialization. Accordingly, a model having land-sea contrast can be integrated from an initial condition in which the boundary layer structure over land is different from that over ocean. Different conditions over urban and rural area can be dealt with, too. Another external factor to influence the boundary layer flow is topography. Its effect may be similarly incorporated in an initialized wind field if the mass field in the mountain region can be specified.

*Acknowledgments.* The authors would like to express thanks to Drs. T. Gordon, K. Miyakoda, B. Ross and I. Simmonds for reviewing and making valuable comments on the manuscript. They also appreciate the useful comments by the reviewers. Thanks are also due to Mrs. B. Williams for typing the manuscript and to Messrs. P. Tunison and J. Conner for preparing the figures.

REFERENCES

Anthes, R. A., 1974: Data assimilation and initialization of hurricane prediction models. *J. Atmos. Sci.*, **31**, 702–719.

Krishnamurti, T. N., 1969: An experiment on numerical weather prediction in equatorial latitudes. *Quart. J. Roy. Meteor. Soc.*, **95**, 594–620.

Kurihara, Y., and J. L. Holloway, 1967: Numerical integration of a nine-level global primitive equation model formulated by the box method. *Mon. Wea. Rev.*, **95**, 509–530.

——, and R. E. Tuleya, 1974: Structure of a tropical cyclone developed in a three-dimensional numerical simulation model. *J. Atmos. Sci.*, **31**, 893–919.

Mesinger, F., 1972: Computation of the wind by forced adjustment to the height field. *J. Appl. Meteor.*, **11**, 60–71.

Miyakoda, K., and R. W. Moyer, 1968: A method of initialization for dynamical weather forecasting. *Tellus*, **20**, 115–128.

——, J. C. Sadler and G. D. Hembree, 1974: An experimental prediction of the tropical atmosphere for the case of March 1965. *Mon. Wea. Rev.*, **102**, 571–591.

——, L. Umscheid, D. H. Lee, J. Sirutis, R. Lusen and F. Pratte, 1976: The near-real-time, global, four-dimensional analysis experiment during the GATE period, Part I. *J. Atmos. Sci.*, **33**, 561–591.

Nitta, T., and J. B. Hovermale, 1969: A technique of objective analysis and initialization for the primitive forecast equations. *Mon. Wea. Rev.*, **97**, 652–658.

Phillips, N. A., 1957: A coordinate system having some special advantages for numerical forecasting. *J. Meteor.*, **14**, 184–185.

Sasaki, Y., 1970: Some basic formalisms in numerical variational analysis. *Mon. Wea. Rev.*, **98**, 875–883.

Sundqvist, H., 1975: Initialization for models using sigma as the vertical coordinate. *J. Appl. Meteor.*, **14**, 153–158.

Winninghoff, F. J., 1973: Note on a simple, restorative-iterative procedure for initialization of a global forecast model. *Mon. Wea. Rev.*, **101**, 79–84.